



**HAL**  
open science

## Dynamic Measurements and Control of an Accelerator Driven System (ADS)

G. Aliberti, G. Rimpault, R. Jacqmin, Jean-Francois Lebrat, P. Finck, Imel G., Andrei Rineiski, Piero Ravetto, J.C. Sens

► **To cite this version:**

G. Aliberti, G. Rimpault, R. Jacqmin, Jean-Francois Lebrat, P. Finck, et al.. Dynamic Measurements and Control of an Accelerator Driven System (ADS). PHYSOR 2002 - International Conference on the New Frontiers of Nuclear Technology: Reactor Physics, Safety and High-Performance Computing, Oct 2002, Seoul, South Korea. cea-02906378

**HAL Id: cea-02906378**

**<https://cea.hal.science/cea-02906378>**

Submitted on 24 Jul 2020

**HAL** is a multi-disciplinary open access archive for the deposit and dissemination of scientific research documents, whether they are published or not. The documents may come from teaching and research institutions in France or abroad, or from public or private research centers.

L'archive ouverte pluridisciplinaire **HAL**, est destinée au dépôt et à la diffusion de documents scientifiques de niveau recherche, publiés ou non, émanant des établissements d'enseignement et de recherche français ou étrangers, des laboratoires publics ou privés.

## Dynamic Measurements and Control of an Accelerator Driven System (ADS)

**G. Aliberti<sup>1</sup>**, G. Rimpault, R. Jacqmin, J.F. Lebrat  
*Commissariat à l'Energie Atomique, Centre d'Etudes de Cadarache*  
*Département d'Etude des Réacteurs, Service de Physique des Réacteurs et du Cycle,*  
*13108 Saint Paul lez Durance Cedex, FRANCE*

<sup>1</sup>Currently at Argonne National Laboratory - USA

*E-Mail: aliberti@ra.anl.gov*

*Phone: +1 630 252 7258*

*Phax: +1 630 252 4500*

P.J. Finck, G. Imel  
*Argonne National Laboratory*  
*Reactor Analysis and Engineering Division*  
*9700 S. Cass Avenue*  
*Argonne, IL 60434 USA*

A. Rineiski  
*Forschungszentrum Karlsruhe,*  
*Institute for Nuclear and Energy Technologies (FZK/IKET),*  
*D-76344 Eggenstein-Leopoldshafen, GERMANY*

P. Ravetto  
*Torino Polytechnic Institute*  
*Dipartimento di Energetica*  
*Corso Duca degli Abruzzi, 24*  
*10100 Torino, ITALY*

J.C. Sens  
*Univerité Louis Pasteur Strasbourg*  
*Institut de Recherches Subatomiques*  
*24 Rue de Loess*  
*67000 Strasbourg, FRANCE*

### Introduction

The existence of Pu and MA stockpiles accumulated over the years by the operation of existing reactors is a matter of public concern. Different options are envisaged to eliminate these stockpiles through burning and transmutation, one of them being the use of ADS (for Accelerator Driven System). A core heavily loaded with Pu and MA is having its safety margins much reduced. A subcritical core driven by an accelerator generating protons which produce neutrons through a spallation process is recovering some of the safety margins which were lacking.

Such complex systems bring with them many particularities which need to be addressed correctly. One of these is to ensure the operators that the reactivity level remains subcritical during the operation of an ADS. Various ideas exist to measure the subcriticality level without becoming critical but this cannot be done without an experimental proof of these possibilities. In order to answer these concerns, this paper is presenting the analysis of the dynamic measurements performed in the MUSE experimental programme and the uncertainty analysis in support of the different techniques envisaged to monitor the subcriticality level during the operation of an ADS. This experimental program called MUSE (for Multiplication of an External Source) has undergone various phases which started in 1995 at CEA in collaboration with CNRS, EdF and Framatome in the MASURCA facility.

In MUSE-3, a small 14-MeV neutron generator was placed at the centre of a sodium-cooled PuO<sub>2</sub>-UO<sub>2</sub> subcritical core in the MASURCA facility. The Pu-to-U+Pu fraction in the fuel was ~25%. Five different subcritical configurations were studied, as well as two additional configurations including a 10-cm-thick lead or sodium buffer placed around the generator. Measurements included reactivity, U-235 fission rates across various traverses and relative source importance. Dynamic measurements were also performed with the generator working in the pulsed mode in order to test a method of reactivity determination using the Pulsed Neutron Source technique.

The aim of this paper is to present the analysis of the dynamic measurement in order to investigate the different techniques to monitor the subcriticality level during the operation of an ADS.

In order to achieve that goal, this paper is presenting:

- the computational tools used for the analysis of these systems and in particular the 3D kinetic module KIN3D of the ERANOS neutronic code system,
- the analysis of the MUSE dynamic measurements,
- the uncertainty evaluation of the dynamic characteristics,
- the assessment of a control system for an ADS.

A conclusion is recalling the various progresses of this study and the remaining aspects to address before effectively designing a reliable control system for an ADS.

## I. The ERANOS code system with its spatial kinetic module KIN3D

The ERANOS fast reactor data and code system [1] includes all required options for calculating fast power reactors as well as MASURCA experimental configurations such as the MUSE cores. The ERANOS reference calculation scheme is based on the ECCO [2] cell/lattice code (Collision Probability Method in many groups using the Sub-group Method), the TGV/VARIANT [3] 3-D transport code (Nodal Variational Method) and the BISTRO [4] code (Optimized Two Dimensional Sn Transport Code). There are perturbation and sensitivity modules in ERANOS associated with the BISTRO Sn transport code. These modules enable calculations within the framework of Classical Perturbation Theory or Generalized Perturbation Theory. Recently the 3D kinetic module KIN3D [5] with associated a new perturbation theory option was developed for the TGV code.

Two sets of nuclear data libraries are available with ERANOS, both of them based on the JEF-2.2 evaluated file [6]. The first set is directly derived from JEF-2.2, whereas the second set, called ERALIB1 [7], is the result of a nuclear data statistical adjustment procedure. The experimental basis for the adjustment is provided by a large number of values (more than 300) measured in clean critical cores.

The treatment of the time dependence in the kinetic module KIN3D is based on two main models: point and space-time kinetics schemes. The starting point is the time-dependent direct neutron transport equation [8], which in its general form is:

$$\begin{aligned} \frac{1}{v} \frac{\partial \Phi_S(\vec{r}, E, \vec{\Omega}, t)}{\partial t} + \vec{\Omega} \cdot \vec{\nabla} \Phi_S + \Sigma(\vec{r}, E, t) \Phi_S = \iint \sum_{x \neq f} \Sigma_x(\vec{r}, E, t) f_x(\vec{r}, E', \vec{\Omega}' \rightarrow E, \vec{\Omega}, t) \Phi_S(\vec{r}, E', \vec{\Omega}', t) dE' d\vec{\Omega}' + \\ + \iint \tilde{\chi}_p(\vec{r}, E') [1 - \beta(\vec{r}, E')] \nu(\vec{r}, E') \Sigma_f(\vec{r}, E', t) \Phi_S(\vec{r}, E', \vec{\Omega}', t) dE' d\vec{\Omega}' + \sum_{j=1}^6 \lambda_j C_j(\vec{r}, t) \tilde{\chi}_j(\vec{r}, E) + S(\vec{r}, E, \vec{\Omega}, t) \quad \text{Eq. 1} \\ \frac{\partial C_j(\vec{r}, t)}{\partial t} + \lambda_j C_j(\vec{r}, t) = \iint \beta_j \nu(\vec{r}, E') \Sigma_f(\vec{r}, E', t) \Phi_S(\vec{r}, E', \vec{\Omega}', t) dE' d\vec{\Omega}' \quad j = 1, \dots, 6 \end{aligned}$$

with:

$\Phi_S(\vec{r}, E, \vec{\Omega}, t)$  : the angular flux;

$S(\vec{r}, E, \vec{\Omega}, t)$ : the external source;

$C_j(\vec{r}, t)$ : the concentration of delayed neutrons precursor for the family j;

$f_x(\vec{r}; E', \vec{\Omega}' \rightarrow E, \vec{\Omega}; t)$ : the probability density that a neutron with direction  $\vec{\Omega}'$  and energy  $E'$  after collision of the type  $x$  get the direction  $\vec{\Omega}$  and energy  $E$ ;  
 $\Sigma(\vec{r}, E, \vec{\Omega}, t)$ ,  $\Sigma_f(\vec{r}, E, \vec{\Omega}, t)$ ,  $\Sigma_{x, x \neq f}(\vec{r}, E, \vec{\Omega}, t)$ : respectively the total, the fission and the “ $x$ ” ( $x$  stands for elastic, inelastic,  $(n, 2n)$ , etc.) macroscopic cross section;  
 $\nu(\vec{r}, E')$ : the average neutron number from a fission in the position  $\vec{r}$  produced by a neutron with energy  $E'$ ;  
 $\tilde{\chi}(\vec{r}, E') = \frac{\chi(\vec{r}, E')}{4\pi}$ : the fission spectrum per solid angle unit;  
 $\beta(\vec{r}, E') = \sum_{j=1}^6 \beta_j(\vec{r}, E')$ : the total delayed neutron fraction.

To obtain the point-kinetic equations one usually introduces the space-time factorisation:

$$\Phi_S(\vec{r}, E, \vec{\Omega}, t) = P(t) \cdot \Psi(\vec{r}, E, \vec{\Omega}, t) \quad \text{Eq.2}$$

where:

- $P(t)$  is the flux amplitude that includes the most part of the time dependence. It determines the power level of the system during the transient;
- $\Psi(\vec{r}, E, \vec{\Omega}, t)$  is the flux shape function, that change very slowly during the transient and take in account the spatial flux distribution.

Combining **Eq.1** with the equation for the adjoint flux  $\Phi_0^*(\vec{r}, E, \vec{\Omega}, t)$  and taking in account the factorisation as shown in **Eq.2**, we obtain the point-kinetic equations:

$$\begin{aligned} \frac{dP(t)}{dt} &= \frac{\rho(t) - \hat{\beta}(t)}{\Lambda(t)} P(t) + \sum_{j=1}^6 \lambda_j c_j(t) + Q(t) \\ \frac{dc_j(t)}{dt} &= \frac{\hat{\beta}_j(t)}{\Lambda(t)} P(t) - \lambda_j c_j(t) \quad j = 1, \dots, 6 \end{aligned} \quad \text{Eq.3}$$

with:

$$\hat{\beta}(t) = \frac{1}{F} \int \dots \int \tilde{\chi}_d(\vec{r}, E) \vec{\beta}_j(\vec{r}, E) \nu(\vec{r}, E') \Sigma_f(\vec{r}, E', t) \Psi(\vec{r}, E', \vec{\Omega}', t) \cdot \Phi_0^*(\vec{r}, E, \vec{\Omega}, t) d\vec{r} dE d\vec{\Omega} dE' d\vec{\Omega}' = \sum_{j=1}^6 \hat{\beta}_j(t) \quad \text{the total effective}$$

delayed neutron fraction;

$$\Lambda(t) = \frac{1}{F} \iiint \frac{1}{v} \Psi(\vec{r}, E, \vec{\Omega}, t) \cdot \Phi_0^*(\vec{r}, E, \vec{\Omega}, t) d\vec{r} dE d\vec{\Omega} : \text{the generation time};$$

$$c_j(t) = \frac{1}{\Lambda(t)F(t)} \iiint \tilde{\chi}_j(\vec{r}, E) C_j(\vec{r}, E, t) \cdot \Phi_0^*(\vec{r}, E, \vec{\Omega}, t) d\vec{r} dE d\vec{\Omega} : \text{the effective concentration of delayed neutrons precursor for the family } j;$$

$$Q(t) = \frac{1}{\Lambda(t)F(t)} \iiint S(\vec{r}, E, \vec{\Omega}, t) \cdot \Phi_0^*(\vec{r}, E, \vec{\Omega}, t) d\vec{r} dE d\vec{\Omega}$$

$$F(t) \text{ standing for } F(t) = \int \dots \int \tilde{\chi}(\vec{r}, E) \nu(\vec{r}, E') \Sigma_f(\vec{r}, E', t) \Psi(\vec{r}, E', \vec{\Omega}', t) \cdot \Phi_0^*(\vec{r}, E, \vec{\Omega}, t) d\vec{r} dE d\vec{\Omega} dE' d\vec{\Omega}'$$

In the point-kinetic model the flux shape is supposed to be constant during the transient.

$$\Phi_S(\vec{r}, E, \vec{\Omega}, t) = P(t) \cdot \Psi(\vec{r}, E, \vec{\Omega}, t = 0)$$

The point-kinetics equations get a simplified form with the time-independent kinetic parameters  $\hat{\beta}$  and  $\Lambda$ .

In the point-kinetic model two time grids are employed by the KIN3D code: a coarse one for the reactivity calculations, associated with a reactivity step, and a fine one for the integration of the point-kinetic equations, associated with an amplitude step.

The point kinetics model is computationally efficient and can provide accurate results for small reactor perturbations when one may assume that the real time-dependent distribution of the power is close to its

steady-state distribution. This model is not suited however for the analysis of large reactor perturbation when a time-dependent flux shape may significantly change compared to the steady-state conditions. For such cases the space-time kinetic methods should be employed in order to obtain more accurate results.

Three main methods are used in KIN3D for the space-time kinetic calculations: the direct method and the adiabatic and the improved quasi-static space-time factorisation schemes.

The direct method uses a straightforward discretisation of the time-dependent neutron transport (or diffusion) equation along the time variable. The discretisation is performed with the implicit scheme, which is mostly recommended for solving in general the neutron kinetic problem due to its numerical stability. When the implicit scheme is used, the time-dependent transport (or diffusion) equation is transformed into a sequence of neutron transport (or diffusion) problems of the steady-state type with an “artificial” external source term.

In the adiabatic and the improved quasi-static space-time factorisation the flux shape is periodically updated by using three time grids: a coarse one for the flux shape calculation (associated with a shape step), an intermediate one for the reactivity calculations (associated with a reactivity step), and a fine one for the integration of the point-kinetic equations (associated with an amplitude step). The two methods are based on the assumption that the flux shape is constant within the shape step and the flux amplitude  $P(t)$  represents a rapidly varying factor in this step. In this way, the point-kinetic method can be also considered as a space-time factorisation scheme with an extremely large shape step.

According to the adiabatic scheme the flux shape is updated by solving the neutron steady-state transport (or diffusion) equation at the beginning of each shape step, where the cross sections are recalculated with the assumption that they change linearly during the transient.

According to the improved quasi-static scheme the flux shape is updated at the end of each shape step, by using the direct method within the shape step.

Each space-time kinetics option has its advantages and disadvantages. The advantage of the direct method is the relative simplicity in the management of the equations (there is no need of the perturbation theory calculation which require additional computations of the adjoint steady-state flux) and an acceptable performance for relatively slow transients in thermal reactors. The disadvantage is the requirement of extremely fine time steps for simulations of certain transients, particularly in the fast reactors.

For such cases the improved quasi-static scheme usually shows a significantly better performance without any loss of accuracy. The management of the equations, however, is more complicated than that for the direct method, the adjoint and the perturbation theory calculations being necessary.

Compared with the improved quasi-static method, the adiabatic scheme has a similar time (shape) step performance and computational costs (usually better than the direct method), but it may be reliably employed for a restricted number of situations. If the transient is provided by an external source change, without any impact on the cross sections, the solution obtained by this scheme is the same than using the point-kinetic model.

## II. The analysis of MUSE3 dynamic measurements

The MUSE-3 [9] experiments consisted of a commercial  $(d,t)$  14 MeV neutron generator placed in a standard MASURCA subassembly loaded at the core center of different subcritical configurations, the tritium target being located at the core midplane. These subcritical configurations were made of  $\text{UO}_2\text{-PuO}_2$  fuel (Pu enrichment  $\approx 25\%$ ) with sodium. In such cores, neutrons from spontaneous fissions and  $(\alpha,n)$  reactions create an inherent source in the subcritical core, inducing a «background» power.

The MUSE-3 experiments started with a critical reference core followed by three subcritical configurations called SC1, SC2 and SC3 of about -500, -1000 and -1500 pcm respectively, which were obtained by unloading peripheral MASURCA subassemblies from the critical reference, as indicated in **Figure 1**. Some measurements were performed with the generator wrapped in a 1 mm thick cadmium layer, to prevent the

thermal neutrons coming from the generator's light materials from re-entering the core (MUSE-3 Cd configuration). In a later phase, the neutron generator was surrounded successively by sodium and pure lead buffers of about 10-cm thickness to simulate the presence of a spallation region and to modify the importance of the 14 MeV neutrons emitted by the generator. In these two configurations, MUSE-3 Pb and MUSE-3 Na, a subcriticality level of about - 5500 pcm was obtained by adjusting the external fuel loading as indicated in **Figure 2**.

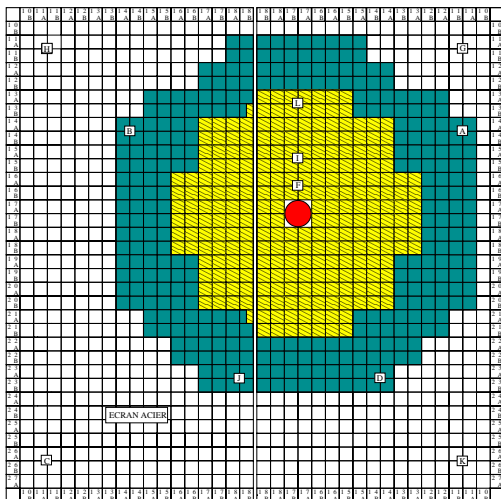
The measured subcritical level, obtained by MSM method, for each configuration is shown in the following table:

Table I

Configuration	$\rho$ [pcm]
MUSE-3 REF	-41
MUSE-3 SC1	-467
MUSE-3 SC2	-1202
MUSE-3 SC3	-1579
MUSE-3 Cd	-2151
MUSE-3 Na	-5893
MUSE-3 Pb	-5687

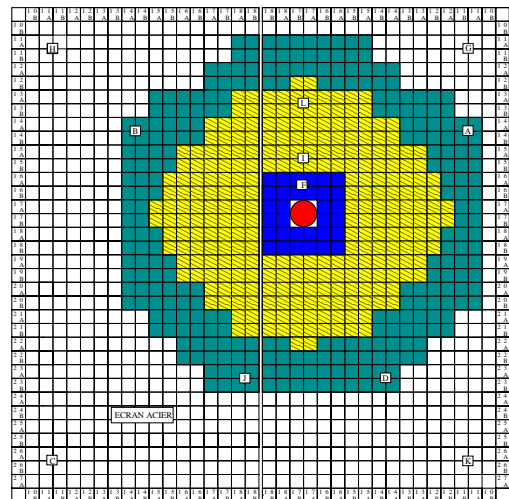
The calculated reactivity values agree with the experimental ones within the margins of uncertainty.

The main difficulty of the MUSE-3 experiment analysis essentially came from the hydrogenated materials present in the (*d-t*) neutron generator in non-negligible quantities which were not specified by the constructor. Notwithstanding this, the analysis was satisfactory. The main conclusions drawn from the steady-state measurements are given in the Ref.10 and 11.



A à A = Positions des compteurs

Figure 1: XY View of the MUSE-3 REF Configuration.



A à A = Positions des compteurs

Figure 2: XY View of the MUSE-3 Pb Configuration.

## II.1 Dynamic Measurements

In each subcritical configuration, measurements were performed with the generator working in the pulsed mode in order to test a method of reactivity determination using the Pulsed Neutron Source technique. In fact, according with the point-kinetic theory the evolution of the system after a swift injection of neutrons by the external source, is approximately described by the equation:

$$P(t) = P_0 e^{-\alpha t} \quad \text{Eq.4}$$

with:  $\alpha = \frac{\hat{\beta} - \rho}{\Lambda}$

It was supposed that a reactor of small dimensions such as MASURCA was suitable for these kinds of studies.

According to the theoretical developments, we are interested in the value of the pulsation  $\alpha$  of the exponential decay. For this reason, in the following we represent always the dynamic behaviour  $P(t)$  in logarithmic scale, normalised at the max value it attains during the transient. In this way, the exponential decay will be described by a straight line, from which one can determine the alpha value.

The frequency was set to 200Hz, and each burst contained about  $10^6$  neutron.  $^{235}\text{U}$  and  $\text{BF}_3$  chambers were connected to an analyser ( $5\mu\text{s}/\text{channel}$ ) recording the counting rate evolution after each burst, for several hundred thousands sweeps. These measurements were performed with the detector F, I, L located in the core region and the detector D located in the reflector region, as shown in the **Figure 1** and **2**.

The reactivity dependence of these decay measurements is shown in the **Figure 3**, where we have plotted the evolution of the F monitor counting rate for different subcritical configurations.

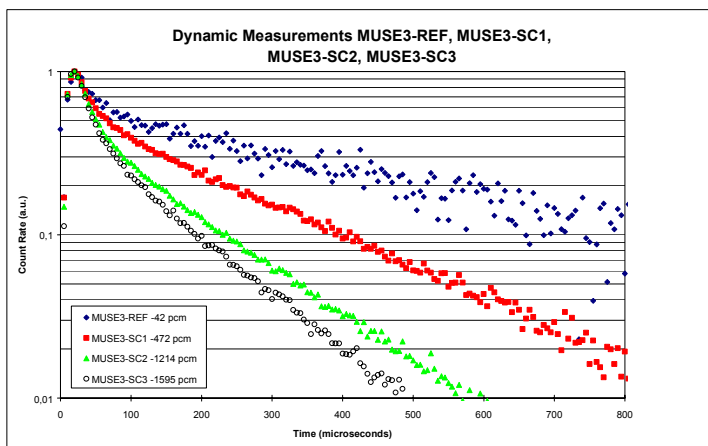


**Figure 3:** Dynamic measurements for the configurations without buffer

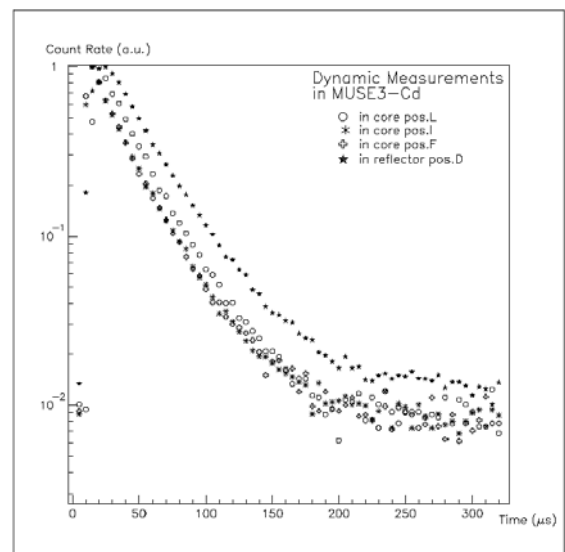


**Figure 4:** Dynamic measurements for MUSE-3 Cd

The most important observation is that the more subcritical the system is, the faster the decay of the counting rate is, according to well known reactor physics.

It is remarkable that in the counting rate the decrease follows two exponentials. The first (“fast”) decay corresponds to fast multiplication of the neutrons injected by the generator, whereas the second one (“slow”) decay corresponds to some multiplication neutrons thermalized by the light materials ( $\text{CH}_2$  used for High Voltage isolation) contained in the generator and whose lifetime is increased.

The counting rate drops to a constant level - corresponding to the inherent source - after a few hundred microseconds, which is very fast. The decay of delayed neutrons cannot be observed on this time scale, the fastest delayed neutron group decaying in about 0.2 s.

For the same configuration, the space dependence of the decay measurements is shown in the **Figure 4**, where we have plotted the evolution of the F, I, L and D monitor counting in the MUSE-3 Cd configuration. The results are the following ones:

Monitor	F	I	L	D
$\alpha$ [Hz]	$39472 \pm 10$	$39933 \pm 10$	$36583 \pm 10$	$30510 \pm 10$

A fit was performed on these measurements using a standard maximum likelihood method, and the monitors-average decay was determined as in **Eq. 4**. The fit result, including all the monitors, is  $\alpha = 38662 \pm 2000$  Hz, which was compared to the first order contribution given by the reactor point-kinetics  $\alpha = \frac{\hat{\beta} - \rho}{\Lambda} = 40484 \pm 2000$  Hz, giving a value for the generation time  $\Lambda = 0.62 \pm 0.03 \mu\text{s}$  and assuming  $\hat{\beta} = 359$  pcm.

The behavior of the monitors located at different positions inside the core (F, I, L) is identical, showing a first order point-kinetic behavior of the reactor.

The monitor D located in the reflector follows a slightly different decay as the core monitors, since the energy spectrum in this region is degraded.

**Figure 6** shows the same plot for the MUSE-3 Pb configuration, where this effect is enhanced for the monitor J - also located in the reflector - since the BF3 chamber in this case is particularly sensitive to spectrum variations. As for the monitor F - located inside the lead buffer - its sensitivity to the neutrons thermalized by the CH2 in the generator is emphasized.

With and without the generator wrapped in a 1 mm thick cadmium layer, the result of the dynamic measurements are compared in **Figure 5**. In MUSE-3 Cd the counting rate evolution follows one exponential only, proving that the two exponentials measured on the other configurations (for example MUSE3-SC3, which has almost the same subcritical level as MUSE-3 Cd) are related to the hydrogenated materials present inside the neutron generator.

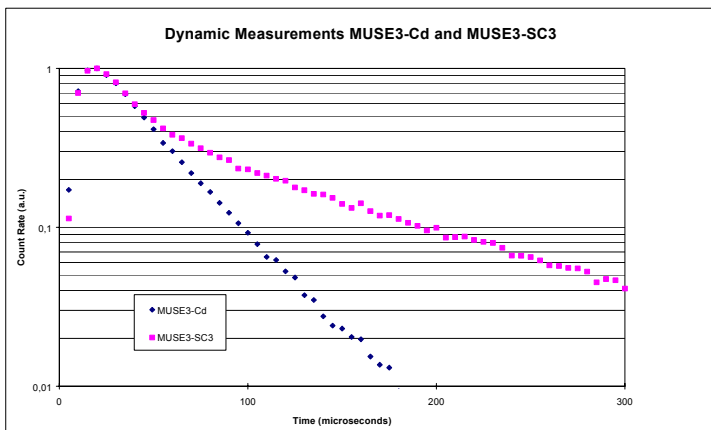


**Figure 5:** Dynamic measurements with cadmium

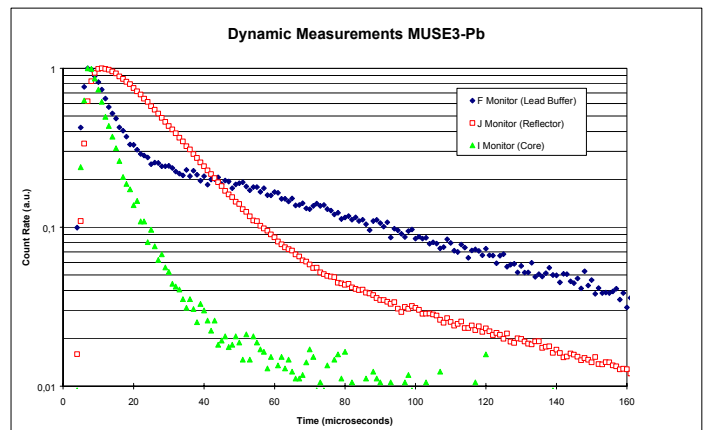


**Figure 6:** Dynamic measurements with buffer

## II.2 Analysis of the dynamic measurement with KIN3D

A first numeric validation of the KIN3D code allowed the analysis of the MUSE-3 dynamic measurements by using both the point-kinetic and the space-time kinetic (the direct method and the improved quasi-static space-time factorisation scheme) methods for solving the point-kinetics equations.

We studied the exponential decay  $P(t)$  of the neutron population after a burst  $S(t)$  of the external source. The injections are modelled by a linear variation of the external source intensity from the value corresponding to the constant level due to the inherent source, up to a maximal value, followed by a symmetric decrease to the initial value. These simulations don't take in account any static fluctuation, which in the practice are associated with every recording.

As the flux amplitude  $P(t)$  depends strongly on the subcriticality level (mainly if we are close to the criticality), in order to allow a comparison between the experimental and the calculated results, the dynamic calculations are performed by normalising the reactivity in the configuration MUSE-3 REF, SC1, SC2, SC3 at the measured value MSM, as shown in the **Table I**. This normalisation was omitted for the MUSE-3 Cd configuration.

A first step concerned the application of the point-kinetic method to the MUSE3 Cd configuration, where the absence of the thermal neutron due to the generator's light materials avoid the spatial effects observed in the other configurations. The calculated and measured comparison for  $P(t)$  is shown in the **Figure 7**.

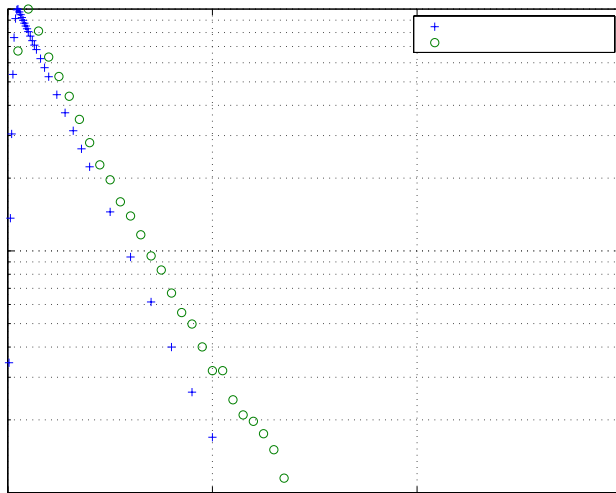


**Figure 7:** MUSE-3 Cd – KIN3D point

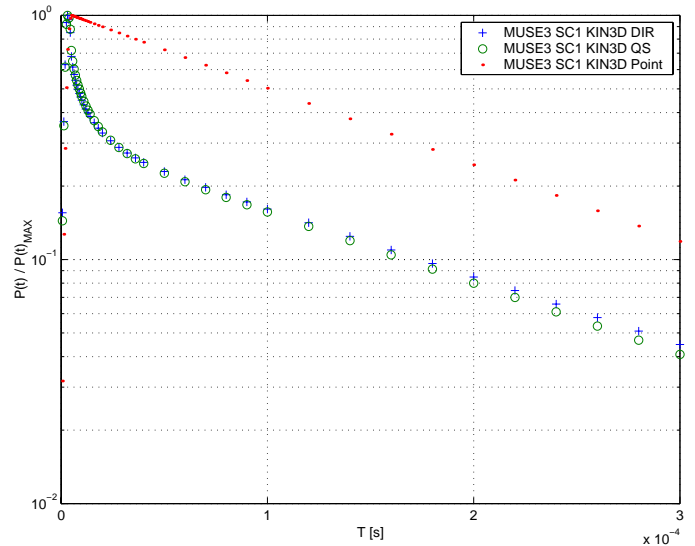


**Figure 8:** MUSE-3 SC1 – methods comparison in the detector F

The ERANOS calculation performed with the simple point-kinetics approximation gave a value of  $\alpha=39908\pm 4000\text{Hz}$  that is comparable with the first order contribution given by  $\alpha=(\hat{\beta}-\rho)/\Lambda$ , which was  $40350\text{Hz}$  with the calculated values  $\Lambda = 0.57 \mu\text{s}$ ,  $\hat{\beta}=359 \text{ pcm}$ ,  $\rho = -1941 \text{ pcm}$ . The uncertainty on the calculated value (see Section III) of  $\alpha$  has been obtained using the ERALIB1 adjusted library with uncertainties in the delayed neutron fraction  $\delta\hat{\beta} = 6\%$ , in the lifetime  $\delta\Lambda = 1.89\%$  and in the reactivity  $\delta\rho=11.39\%$ . Therefore, with the ERALIB1 library, dynamic calculation results showed a good agreement with the experimental ones ( $\alpha=39933\pm 10\text{Hz}$  for the Monitor I in the core, or  $\alpha=38662\pm 2000\text{Hz}$  from the fit procedure; see Section II.1) and this with quite small uncertainties.

The use of unadjusted cross sections JEF2, producing large uncertainty on the reactivity value (about 70%), would have, however, lead to an unacceptably large uncertainty in  $\alpha$ . That kind of uncertainty is representative of a situation which would prevail if a subcritical core were to be loaded with dedicated fuels, heavily loaded with Minor Actinides with badly known cross sections. In this case it would be suitable to use the experimental reactivity MSM, which introduces small uncertainty on the reactivity value.

The point-kinetic method is not suitable to analyse the dynamic measurements in the other configurations, where the counting rate decrease follows two exponentials. As shown in the **Figure 8**, the point-kinetic approximation is unable to describe the first (“fast”) decay corresponding to the fast multiplication of the neutrons injected by the generator, thermalized by the light materials contained in the generator and whose lifetime is increased. For this kind of study we need to use any of space-time kinetic methods, the direct method and the improved quasi-static space-time factorisation scheme giving the same results.

The following figures have been obtained by using the direct method. The **Figure 9** shows the counting rate decay recorded in the detector F for each configuration. The **Figure 10** shows the amplitude flux  $P(t)$  in the different detectors for the MUSE-3 SC1 configuration.

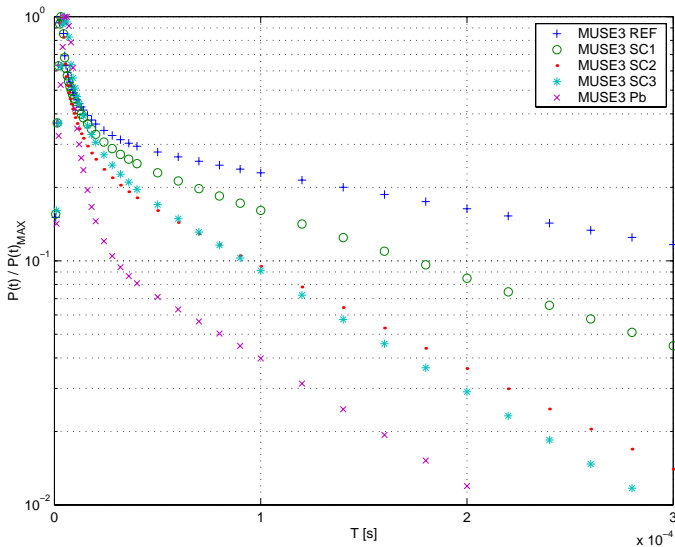


**Figure 9:** KIN3D direct method – detector F

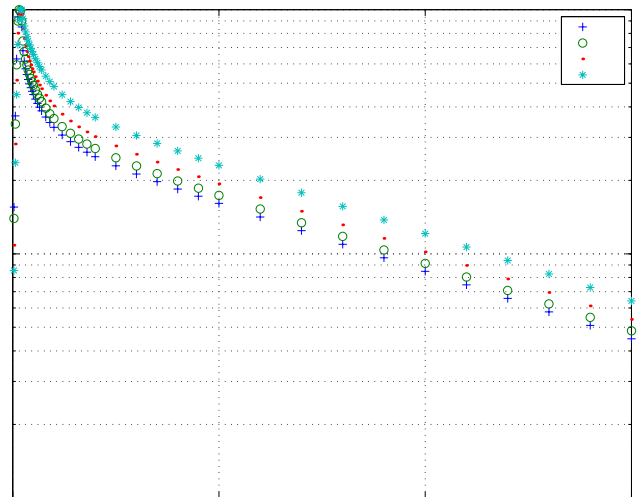


**Figure 10:** MUSE-3 SC1 – KIN3D direct method

All the conclusions drawn for the experimental measurements, concerning the dynamic dependence on the subcritical level and on the detector location (core or reflector region) are confirmed by the calculation.

Concerning the comparison of the calculated decay with the measured one, the **Figures 11** and **12** show together, as example, the two behaviours of the detector F in the MUSE-3 SC1 and MUSE-3 Pb configuration.

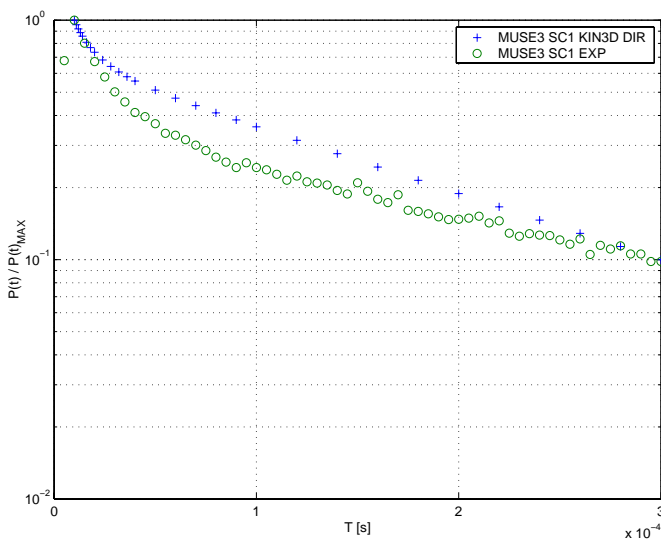


**Figure 11:** MUSE-3 SC1 – Exp. and Calc. results

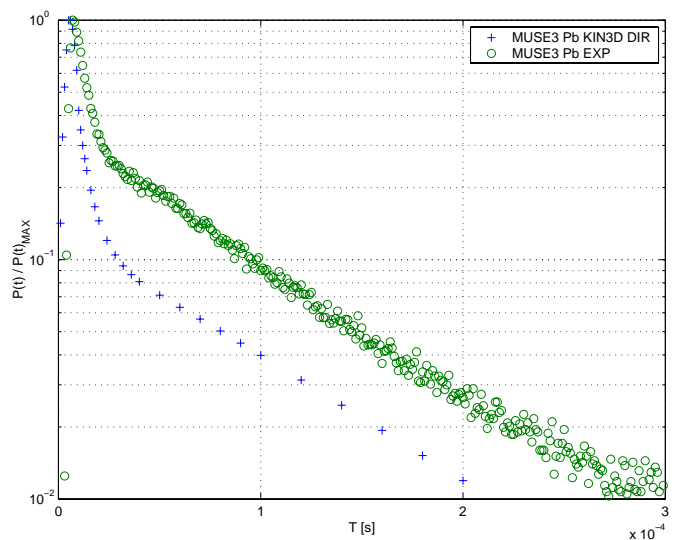


**Figure 12:** MUSE-3 Pb – Exp. and Calc. results

Right away we can observe that the two decays  $P(t)$ , the calculated and the experimental one, are quite different at the beginning of the transient, soon after the burst  $S(t)$ . The subsequent behaviour shows that this difference is decreasing. In order to quantify the discrepancies, if we call  $\alpha_1$  the exponential characterising the first “fast” decay at the begin of the transient, and  $\alpha_2$  the second “slow” decay, in the MUSE3-SC1 case (**Figure 12**) we found:

$$\alpha_{1,\text{exp}} = 31554 \pm 1640 \text{ Hz}; \alpha_{2,\text{exp}} = 950.4 \pm 49 \text{ Hz}$$

$$\alpha_{1,\text{calc}} = 58876 \pm 22020 \text{ Hz}; \alpha_{2,\text{calc}} = 825.3 \pm 309 \text{ Hz}$$

We conclude that the calculated “slow” decay agree with the experimental one within the margins of uncertainty. The comparison is less satisfactory for the first decay. However, the real conditions to compare are more complicated than they appear. First, according to the reactor dynamic equations, we know that at the begin of the transient the decay depends strongly on the shape of the burst  $S(t)$ , of which we have evidence in the calculated case only. We have just an idea about the real evolution  $S(t)$ : some studies performed by the ISN – Grenoble (France) – team, showed that the injections made by the neutron generator are often irregular and sometimes they superpose, what produces a length of the burst longer than the requested one.

There is another important aspect to be considered: at the beginning of the transient the dynamic is very fast, the times are comparable with the generation time (fraction of micro-seconds) as shown in the **Figure 13**, obtained from a zoom of the **Figure 11**.

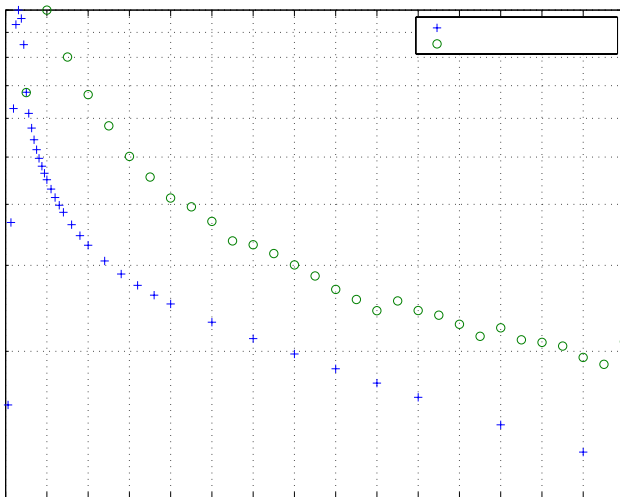


**Figure 13:** MUSE-3 SC1 – Exp. and Calc. results

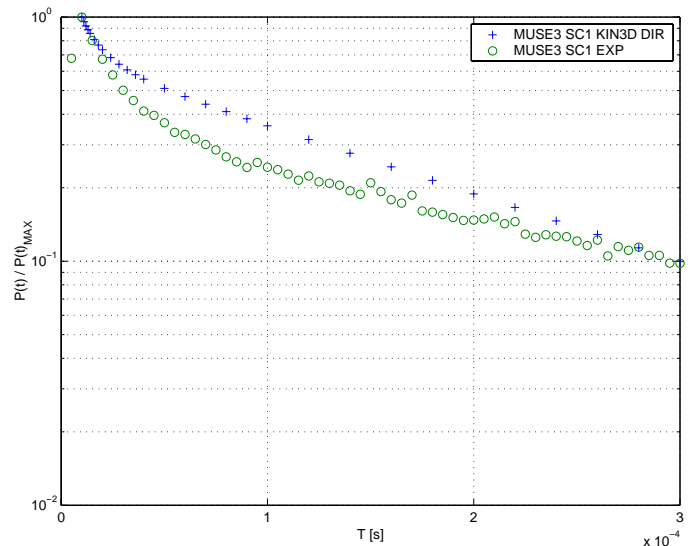


**Figure 14:** MUSE-3 SC1 – Exp. and Calc. results

For the MUSE-3 SC1 the neutron generator produces a burst within the interval  $0 < t < 5 \mu\text{s}$  and the performance of the monitor counting allows to get an answer just every  $5 \mu\text{s}$ , which is a time grid too coarse for such dynamic measurements. In fact, as shown in the **Figure 13**, the maximum value  $P_{\text{MAX}}$  is measured at  $t = 10 \mu\text{s}$ ; if in reality it have been produced at any time  $5 < t < 10 \mu\text{s}$  we lost an important part of the fast decay that happens at beginning of the transient. To fix the ideas, **Figure 14** shows us how would have been the comparison of the experimental and calculated results if we have supposed that  $P_{\text{MAX}}$  was produced at  $t = 10 \mu\text{s}$  in the calculation too. For the first decay we would get:

$$\alpha_{1,\text{exp}} = 31554 \pm 1641 \text{ Hz};$$

$$\alpha_{1,\text{calc}} = 40789 \pm 15255 \text{ Hz};$$

The discrepancy between the calculation and the experiment would be justified by the uncertainty at stake. With this we don't want to justify the calculated results. The aim was to show the importance to use a neutron generator with very high performances, able to produce a burst with a well-known shape. Further the

monitors counting should be able to get an answer with a time step comparable to the generation time that characterize the dynamic behavior.

The lessons drawn from the MUSE-3 experiment was very useful for the next experiment MUSE-4, where an accelerator, called GENEPI, is being used.

### III. Uncertainty evaluation of the dynamic characteristics

The foregoing analysis proved that some dynamic effects could be investigated by a good understanding of the generation time  $\Lambda$ . For this aim, some procedures were developed and implemented in the ERANOS system, for the uncertainty and the spatial dependence calculation.

In a first step we investigated how the generation time changes in the different zones of the reactor. The results are shown in the following table:

Table II: Spatial repartition of  $\Lambda$

	MUSE-3 REF	MUSE-3 Cd	MUSE-3 Pb
Core	3.93E-7	2.93E-7	3.38E-7
Buffer (Pb)	-	-	1.32E-6
Reflector	2.30E-7	2.20E-7	2.65E-7
Radial Shielding	3.54E-9	4.50E-9	1.02E-8
Axial Shielding	1.60E-9	1.61E-9	1.83E-9
Steel (*)	2.45E-7	1.98E-8	1.67E-7
Light materials (*)	4.73E-7	2.04E-8	2.25E-7
Sum	1.35E-6	5.59E-7	2.33E-6

(\*) Generator

First we can observe that  $\Lambda$  attains an important value in the reflector region, which reflects the neutrons in the core after having slowed them down. Among the different configurations, the presence of the buffer makes  $\Lambda$  increase in the MUSE-3 Pb configuration. For the configurations without buffer we can observe the effect of the cadmium layer, that reduces the generation time in the light materials inside the generator by preventing that they reach the core after having been slowed down.

In order to calculate the uncertainties on  $\Lambda$  related to the cross section data, the methodology based on the adaptation of the GPT (Generalized Perturbation Theory) to subcritical source driven systems, and developed in Ref. [10], has been adopted. The ERANOS codes have been used to calculate neutron fluxes, importances, sensitivity coefficients and uncertainty values. JEF2.2 and ERALIB1 cross sections in a 33 group structure have been used for the reference calculations, while the dispersion (variance and covariance data) matrix was in a 15 group structure. The variance dispersion matrix associated to the JEF2.2 Library is shown in Appendix A.

Uncertainty results are summarized in the **Table III** for each configuration and they are broken down by isotopes and cross section type in the **Figures 15 to 17**.

Table III

$\Lambda$ Uncertainty (%)	JEF2.2	ERALIB1
MUSE-3 SC3	22.4	1.7
MUSE-3 Cd	3.3	1.9
MUSE-3 Pb	25.9	6.4

For the MUSE-3 SC3 configuration the total uncertainty on  $\Lambda$  is 22.4% when using JEF2.2 data. The most important contribution is due to the hydrogen cross section, in particular the inelastic and the capture one (**Figure 15**). Using ERALIB1 data, with adjusted cross sections, the total uncertainty is 1.7%.

For the MUSE-3 Cd the 1 mm thick cadmium layer around the generator avoid the thermal effects due to the generator's light materials (**Figure 16**). To total value of uncertainty decreases (3.3% - JEF2.2). With ERALIB1 data the total uncertainty is 1.9%.

For MUSE-3 Pb configuration, the lead contributes (**Figure 17**) with the hydrogen to the total uncertainty (25.9% - JEF2.2). With ERALIB1 data the total uncertainty is 6.4%.

Isotope	$\sigma_{cap}$	$\sigma_{fiss}$	$\nu$	$\sigma_{el}$	$\sigma_{inel}$	$\sigma_{n,2n}$	Total
Pu239	8.3e-3	6.6e-2	2.3e-2	6.9e-4	2.3e-3	3.7e-5	7.1e-2
Pu240	4.7e-3	1.3e-2	4.4e-3	4.1e-4	8.0e-4	1.3e-5	1.4e-2
Pu241	7.0e-4	3.7e-3	6.1e-4	3.3e-5	7.0e-5	1.1e-5	3.9e-3
Pu242	1.5e-4	3.4e-4	1.2e-4	1.7e-5	3.2e-5	1.3e-6	3.9e-4
U235	1.1e-4	1.5e-3	1.3e-4	1.3e-5	2.3e-5	7.5e-7	1.5e-3
U238	4.2e-3	8.5e-3	6.7e-3	1.8e-3	1.0e-2	2.4e-4	1.5e-2
Am241	4.6e-3	2.9e-3	9.8e-4	1.4e-5	2.6e-4	0.0e+0	5.5e-3
Np237	1.7e-9	8.6e-11	3.2e-11	5.7e-12	1.1e-11	0.0e+0	1.7e-9
Fe56	8.1e-3	0.0e+0	0.0e+0	1.9e-2	4.9e-3	0.0e+0	2.2e-2
Fe57	2.5e-4	0.0e+0	0.0e+0	8.6e-4	3.3e-3	0.0e+0	3.4e-3
Cr52	9.7e-4	0.0e+0	0.0e+0	1.1e-2	8.0e-4	0.0e+0	1.1e-2
Ni58	2.0e-3	0.0e+0	0.0e+0	3.4e-3	6.0e-4	0.0e+0	3.9e-3
Na	5.3e-4	0.0e+0	0.0e+0	6.8e-4	1.0e-2	0.0e+0	1.1e-2
H	1.1e-1	0.0e+0	0.0e+0	1.8e-1	0.0e+0	0.0e+0	2.1e-1
Total	1.2e-1	6.8e-2	2.4e-2	1.8e-1	1.6e-2	2.5e-4	2.2e-1

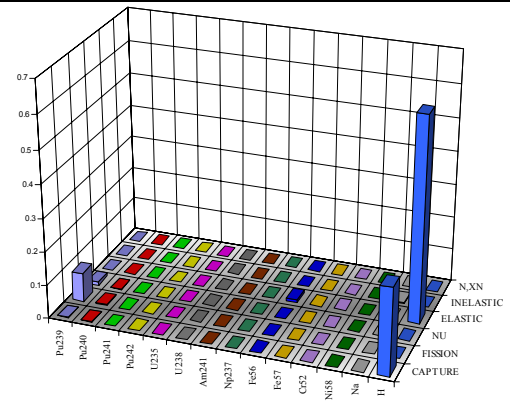


Figure 15: A MUSE-3 SC3 – Uncertainty with JEF2.2 Data – Edition by Isotope

Isotope	$\sigma_{cap}$	$\sigma_{fiss}$	$\nu$	$\sigma_{el}$	$\sigma_{inel}$	$\sigma_{n,2n}$	Total
Pu239	9.9e-3	1.1e-2	1.8e-3	2.3e-4	1.2e-3	9.2e-6	1.5e-2
Pu240	4.3e-3	2.0e-3	5.6e-4	1.5e-4	4.5e-4	4.3e-6	4.8e-3
Pu241	5.0e-4	7.5e-4	1.4e-4	1.2e-5	3.5e-5	2.6e-6	9.2e-4
Pu242	1.7e-4	5.5e-5	1.8e-5	5.8e-6	1.5e-5	3.6e-7	1.8e-4
U235	1.4e-4	3.9e-4	1.7e-5	4.3e-6	1.4e-5	1.1e-7	4.1e-4
U238	2.7e-3	1.3e-3	1.1e-3	6.0e-4	4.5e-3	6.5e-5	5.6e-3
Am241	5.6e-3	4.6e-4	1.6e-4	5.1e-6	1.3e-4	0.0e+0	5.6e-3
Np237	6.0e-9	1.8e-11	7.2e-12	1.9e-12	1.8e-11	0.0e+0	6.0e-9
Fe56	1.1e-2	0.0e+0	0.0e+0	7.0e-3	4.1e-3	0.0e+0	1.4e-2
Fe57	9.1e-4	0.0e+0	0.0e+0	4.1e-4	5.3e-3	0.0e+0	5.4e-3
Cr52	1.8e-3	0.0e+0	0.0e+0	2.3e-3	5.7e-4	0.0e+0	3.0e-3
Ni58	2.3e-3	0.0e+0	0.0e+0	2.3e-3	4.0e-4	0.0e+0	3.3e-3
Cd	1.4e-2	0.0e+0	0.0e+0	1.6e-3	2.3e-5	3.0e-6	1.4e-2
Na	3.1e-4	0.0e+0	0.0e+0	2.0e-3	6.1e-3	0.0e+0	6.4e-3
H	2.0e-3	0.0e+0	0.0e+0	1.7e-2	0.0e+0	0.0e+0	1.7e-2
Total	2.2e-2	1.2e-2	2.2e-3	1.9e-2	1.0e-2	6.6e-5	3.3e-2

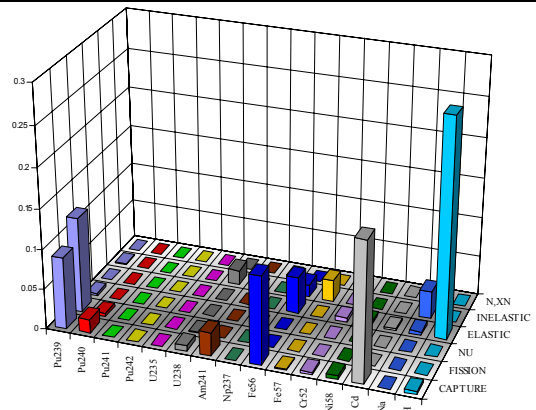


Figure 16: A MUSE-3 Cd – Uncertainty with JEF2.2 Data – Edition by Isotope

Isotope	$\sigma_{cap}$	$\sigma_{fiss}$	$\nu$	$\sigma_{el}$	$\sigma_{inel}$	$\sigma_{n,2n}$	Total
Pu239	4.3e-3	3.3e-2	1.1e-2	2.0e-4	1.4e-3	1.2e-5	3.5e-2
Pu240	2.4e-3	6.3e-3	2.2e-3	1.3e-4	5.0e-4	4.1e-6	7.1e-3
Pu241	3.5e-4	1.9e-3	2.7e-4	9.9e-6	4.3e-5	5.6e-6	1.9e-3
Pu242	9.2e-5	1.7e-4	5.9e-5	5.1e-6	1.9e-5	4.3e-7	2.0e-4
U235	5.5e-5	7.7e-4	5.9e-5	3.7e-6	1.4e-5	3.0e-7	7.7e-4
U238	2.1e-3	4.2e-3	3.4e-3	5.2e-4	6.1e-3	8.3e-5	8.4e-3
Am241	2.8e-3	1.4e-3	4.9e-4	4.2e-6	1.6e-4	0.0e+0	3.1e-3
Np237	5.9e-9	3.5e-11	1.2e-11	8.0e-12	2.2e-11	0.0e+0	5.9e-9
Fe56	1.1e-2	0.0e+0	0.0e+0	1.1e-2	3.2e-3	0.0e+0	1.6e-2
Fe57	2.9e-4	0.0e+0	0.0e+0	5.3e-4	2.0e-3	0.0e+0	2.1e-3
Cr52	1.2e-3	0.0e+0	0.0e+0	5.6e-3	5.9e-4	0.0e+0	5.8e-3
Ni58	2.0e-3	0.0e+0	0.0e+0	1.9e-3	3.9e-4	0.0e+0	2.8e-3
Cd	4.1e-2	0.0e+0	0.0e+0	3.5e-2	7.4e-3	2.8e-2	6.1e-2
Na	4.6e-4	0.0e+0	0.0e+0	2.7e-4	6.8e-3	0.0e+0	6.8e-3
H	1.4e-1	0.0e+0	0.0e+0	2.0e-1	0.0e+0	0.0e+0	2.5e-1
Total	1.5e-1	3.4e-2	1.2e-2	2.1e-1	1.2e-2	2.8e-2	2.6e-1

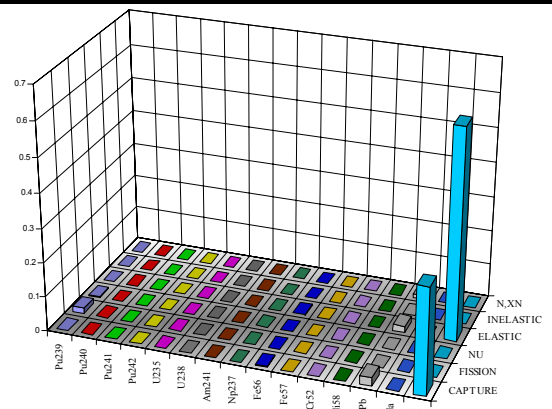


Figure 17: A MUSE-3 Pb – Uncertainty with JEF2.2 Data – Edition by Isotope

#### IV. Assessment of a control system for an ADS

Sensitivity analyses based on the perturbation theory allow us to know in which margin we can get the reactivity measurement by dynamic techniques. In this way we can provide some interesting recommendations about the operation of an ADS, where the integral parameters are affected by a bigger uncertainty due to the presence of Minor Actinides with badly known cross sections.

The MUSE-3 experiment proved that, in absence of anomalous perturbations like light materials effects, the exponential decay  $P(t)$  due to a burst of the external source is well approximated by the law:  $P(t) = P_0 e^{-\alpha t}$ , with  $\alpha = \frac{\hat{\beta} - \rho}{\Lambda}$ . In reality this situation is characteristic of small core (“point reactor”) and it could have some restrictions in the case on the reactor with industrial size, where the spatial effects could be important.

Anyway let’s suppose that the ADS dynamic is of  $e^{-\alpha t}$  type. The reactivity could be determined by the Pulsed Neutron Source technique, as:  $\rho = \hat{\beta} - \alpha\Lambda$ . This method could allow reactivity measurements in a subcritical configuration simply by fitting the counting decay of the monitor, without taking into account any critical “reference” state associated to the configuration under study.

However, particular attention has to be paid to assure that the values obtained are as precise than we have to expect. In fact, if  $I_\alpha$ ,  $I_{\hat{\beta}}$  and  $I_\Lambda$  are respectively the uncertainty associated to  $\alpha$ ,  $\hat{\beta}$  and  $\Lambda$ , the uncertainty on the reactivity  $\rho$  will be:

$$I_\rho = \sqrt{\frac{\hat{\beta}^2}{\rho^2} I_{\hat{\beta}}^2 + \frac{\alpha^2 \Lambda^2}{\rho^2} (I_\alpha^2 + I_\Lambda^2)} \quad \text{Eq.5}$$

We must be sure that the margin of uncertainty on the reactivity is enough to guarantee a correct operation in subcriticality. For example, for the MUSE-3 Cd configuration the foregoing uncertainty analysis allows us to set:  $I_\alpha = 5.2\%$ ,  $I_{\hat{\beta}} = 6\%$  and finally  $I_\Lambda = 3.3\%$ . By using the **Eq. 5** we obtain  $I_\rho = 7\%$ , which is a good margin of uncertainty, as the absolute value of the reactivity is about  $-2000$  pcm. But for the other configurations we observed that the counting decay follows two exponentials: the uncertainties fixed for  $\alpha$  and  $\Lambda$  are more important. This is to point out the importance of the uncertainty methods which have been developed for operating an ADS, mainly the subcritical cores with dedicated fuels, heavily loaded with Minor Actinides.

The fact that detectors in an ADS might be located below the reactor vessel is somehow complicating the picture. The signal detected by fission chambers located far from the core is distorted by the transfer of neutrons through the different media it is crossing.

Although we have been able to reproduce some of the spatial kinetic effects encountered in the MUSE3 program, we have failed to reproduce the spatial kinetic effects of detectors located in the reflector. On the observed calculation-experiment (C-E) discrepancies the impact of the calculation methods is supposed to be negligible compared with the effects related to the experiment (presence of the hydrogenated materials inside the generator), to the measurement techniques (a time step too coarse for the transient under study) and to the generator’s performances (shape of the burst poorly known).

Therefore, unless this problem is solved and in order to minimize the possible hazards which might occur during the transfer of neutrons to the remote detector, it is recommended to place the detector within the core with all associated constraints (such as a high flux level and the high temperature) taken into account.

#### IV. Conclusions

In order to investigate the ADSs physics, an important experimental program has been set up in the MASURCA facility. This experimental program called MUSE (for Multiplication of an External Source) and started in 1995 at CEA in collaboration with CNRS, EdF and Framatome, has undergone various phases. One major step in this program has been the achievement of the MUSE-3 experiment in 1998.

In MUSE-3, a small 14-MeV neutron generator was placed at the centre of a sodium-cooled PuO<sub>2</sub>-UO<sub>2</sub> subcritical core in the MASURCA facility. The Pu-to-U+Pu fraction in the fuel was ~25%. The MUSE-3 experiments started with a critical reference core followed by three subcritical configurations called SC1, SC2 and SC3 of about -500, -1000 and -1500 pcm respectively, which were obtained by unloading peripheral MASURCA subassemblies from the critical reference. Some measurements were performed with the generator wrapped in a 1 mm thick cadmium layer, to prevent the thermal neutrons coming from the generator's light materials from re-entering the core (MUSE-3 Cd configuration). In a later phase, the neutron generator was surrounded successively by sodium and pure lead buffers of about 10-cm thickness to simulate the presence of a spallation region and to modify the importance of the 14 MeV neutrons emitted by the generator. In these two configurations, MUSE-3 Pb and MUSE-3 Na, a subcriticality level of about -4500 pcm was obtained by adjusting the external fuel loading. Measurements included reactivity, U-235 fission rates across various traverses and relative source importance. Dynamic measurements were also performed with the generator working in the pulsed mode in order to test a method of reactivity determination using the Pulsed Neutron Source technique. The dynamic studies have been carried out via the 3D kinetic module KIN3D of the ERANOS neutronic code system.

The main difficulty of the MUSE-3 experiment analysis essentially came from the hydrogenated materials present in the (*d-t*) neutron generator in non-negligible quantities which were not specified by the constructor. Notwithstanding this, the analysis was satisfactory. Another further difficulty arises from the fact that in a power ADS, fission chambers will be located in the reflector or below the reactor vessel. The dynamic measurement is then distorted by spatial effects which need to be addressed correctly. The spatial kinetic code KIN3D with its specifically spatial modes enables the treatment of such effects, measured in some of the MUSE configuration.

For the measurement without cadmium the counting rate decrease follows two exponentials. The first ("fast") decay corresponds to fast multiplication of the neutrons injected by the generator, whereas the second one ("slow") decay corresponds to some multiplication neutrons thermalized by the light materials (CH<sub>2</sub> used for High Voltage isolation) contained in the generator and whose lifetime is increased.

With the generator wrapped in a 1 mm thick cadmium layer, the result of the dynamic measurements follows one exponential only. In this case the calculated results were obtained with the point-kinetic model of the KIN3D code. Using the ERALIB1 library, dynamic calculation results showed a good agreement with the experimental ones and this with quite small uncertainties. However, the use of unadjusted cross sections JEF2.2, producing large uncertainty on the reactivity value (about 70%), leads to an unacceptably large uncertainty in  $\alpha$ . That kind of uncertainty is representative of a situation which would prevail if a subcritical core was to be loaded with fuels having an high content of Minor Actinides with poorly known cross sections. In this case it would be suitable to use the experimental reactivity MSM, which introduces small uncertainty on the reactivity value.

The point-kinetic model is unable to reproduce by the calculation the dynamic behavior for the configuration without cadmium. The presence of two exponential decays was investigated by a space-time method. The study of the discrepancy between the calculation and the experiment allows us to show the importance to use a neutron generator with very high performances, able to produce a burst with a well-known time shape. Further the monitors counting should be able to get an answer with a time step comparable to the generation time that characterizes the dynamic behavior.

The lessons drawn from the MUSE-3 experiment were very useful for the next experiment MUSE-4, where an accelerator, called GENEPI, is being used.

Some interesting conclusions were also drawn on the way to operate an ADS. For these systems, the reactivity could be determined by the Pulsed Neutron Source technique, as:  $\rho = \hat{\beta} - \alpha\Lambda$ . This method could allow reactivity measurements in a subcritical configuration simply by fitting the counting decay of the monitor, without taking into account any critical "reference" state associated to the configuration under study. Special care should be given to the type and the position of the detector in order to get a correct measurement of the subcriticality level and ensure that the margin of uncertainty on the reactivity is enough to guarantee a safe operation of the ADS in a subcriticality mode. This is to point out the importance of the uncertainty methods which have been developed for designing an ADS, especially when the subcritical core uses dedicated fuels, heavily loaded with Minor Actinides.

## References

- [1] G. PALMIOTTI, R.F. BURSTALL, E. KIEFHABER, W. GEBHARDT, J.M. RIEUNIER  
"New Methods Developments and Rationalization of Tools for LMFBR Design in the Frame of the European Collaboration",  
FR'91 International Conference on Fast Reactors and Related Fuel Cycles, Kyoto, Japan, October 28 – November 1, 1991
- [2] G. RIMPAULT  
"Algorithmic Features of the ECCO Cell Code for treating Heterogeneous Fast Reactor Assemblies",  
International Topical Meeting on Reactor Physics and Computation, PORTLAND - OREGON, May 1-5, 1995
- [3] G. PALMIOTTI, C.B. CARRICO and E.E. LEWIS  
"Variational Nodal Transport Methods with Anisotropic Scattering",  
Nucl. Sc. Eng., 115, p.233 (1993)
- [4] G. PALMIOTTI, J.M. RIEUNIER, C. GHO, M. SALVATOIRES  
"BISTRO Optimized Two Dimensional Sn Transport Code",  
Nuclear Science and Engineering, 104, 26 (1990)
- [5] A. RINEISKI, W. MASCHKE, G. RIMPAULT  
Performance of Neutron Kinetics Models for ADS Transient Analyses,  
AccAPP/ADTTA'01, ANS 2001 Winter Meeting November 11-15, 2001, Reno, Nevada, U.S.A.
- [6] OECD/NEA Report 17  
"The JEF-2.2 Nuclear Data Library", April 2000
- [7] E. FORT, W. ASSAL, G. RIMPAULT, J. ROWLANDS, P. SMITH, R. SOULE  
"Realisation and performance of the adjusted nuclear data library ERALIB1 for calculating fast reactor neutronics",  
PHYSOR 96, MITO, JAPAN, September 1996
- [8] G.I. BELL, S. GLASSTONE  
"Nuclear Reactor Theory",  
Litton Educational Publishing, 1970
- [9] J.F. LEBRAT, R. SOULE, M. MARTINI, C.A. BOMPAS, P. BERTRAND, P. CHAUSSONNET, J.P. CHAUVIN, M. SALVATOIRES, G. ALIBERTI, G. RIMPAULT  
"Experimental Investigation of Multiplying Subcritical Media in Presence of an External Source Operating in Pulsed or Continuous Mode: the MUSE-3 Experiment",  
Internal Conference on ADS, PRAGUE, 1999.
- [10] G. ALIBERTI, G. RIMPAULT, R. JACQMIN, J.F. LEBRAT, M. SALVATOIRES, G. PALMIOTTI, J. VERGNES, P. BARBRAULT, D. VERRIER, B. CARLUEC  
"Uncertainty Assessment for Subcritical Multiplying Systems and Application to the MUSE-3 Experiment",  
Submitted to Annals of Nuclear Energy
- [11] G. ALIBERTI, G. RIMPAULT, R. JACQMIN, J.F. LEBRAT, R. SOULE, J.P. CHAUVIN, G. GRANGET, M. SALVATOIRES  
"Analysis of the MUSE-3 Subcritical Experiment",  
Int. Conf. Global2001, France, Paris, September 2001

Appendix A: Variance Matrix Associated to the JEF2 Library

		Pu239						Pu240						Np237					Fe56			Fe57			
Gr	E [MeV]	$\nu$	$\sigma_f$	$\sigma_{inel}$	$\sigma_{el}$	$\sigma_{capt}$	$\sigma_{n,2n}$	$\nu$	$\sigma_f$	$\sigma_{inel}$	$\sigma_{el}$	$\sigma_{capt}$	$\sigma_{n,2n}$	$\nu$	$\sigma_f$	$\sigma_{inel}$	$\sigma_{el}$	$\sigma_{capt}$	$\sigma_{inel}$	$\sigma_{el}$	$\sigma_{capt}$	$\sigma_{inel}$	$\sigma_{el}$	$\sigma_{capt}$	
1	7.05	0.008	0.03	0.1	0.05	0.1	0.13	0.012	0.05	0.15	0.1	0.3	0.16	0.05	0.2	0.5	0.05	0.4	0.062	0.1	0.15	0.062	0.1	0.15	
2	2.73	0.0075	0.037	0.1	0.05	0.085	0.25	0.014	0.05	0.15	0.1	0.3	1	0.05	0.2	0.5	0.05	0.4	0.068	0.1	0.1	0.068	0.1	0.1	
3	1.93	0.007	0.037	0.1	0.05	0.095	1	0.018	0.1	0.15	0.1	0.3	1	0.05	0.2	0.5	0.05	0.4	0.056	0.1	0.07	0.056	0.1	0.07	
4	8.21e-1	0.0065	0.065	0.15	0.05	0.13	1	0.02	0.1	0.15	0.1	0.3	1	0.05	0.2	0.5	0.05	0.4	0.2	0.1	0.07	0.2	0.1	0.07	
5	3.02e-1	0.0055	0.04	0.15	0.05	0.13	1	0.028	0.2	0.2	0.1	0.25	1	0.05	0.2	0.5	0.05	0.4	1	0.08	0.07	1	0.08	0.07	
6	1.11e-1	0.008	0.028	0.15	0.05	0.078	1	0.03	0.2	0.2	0.1	0.15	1	0.05	0.2	0.5	0.05	0.4	1	0.06	0.076	1	0.06	0.076	
7	4.09e-2	0.015	0.03	0.2	0.05	0.039	1	0.0312	0.2	0.2	0.1	0.1	1	0.05	0.2	0.5	0.05	0.4	1	0.04	0.08	1	0.04	0.08	
8	1.50e-2	0.008	0.045	0.25	0.05	0.056	1	0.0311	0.2	1	0.1	0.1	1	0.05	0.2	0.5	0.05	0.4	1	0.04	0.08	1	0.04	0.08	
9	3.35e-3	0.008	0.063	0.25	0.05	0.056	1	0.031	0.2	1	0.1	0.1	1	0.05	0.2	0.5	0.05	0.4	1	0.04	0.08	1	0.04	0.08	
10	7.49e-4	0.0051	0.02	1	0.05	0.065	1	0.03	0.2	1	0.1	0.1	1	0.05	0.2	0.5	0.05	0.4	1	0.04	0.08	1	0.04	0.08	
11	4.02e-5	0.005	0.025	1	0.05	0.065	1	0.029	0.2	1	0.1	0.1	1	0.05	0.2	0.5	0.05	0.4	1	0.04	0.08	1	0.04	0.08	
12	8.32e-6	0.003	0.025	1	0.05	0.065	1	0.028	0.2	1	0.1	0.08	1	0.05	0.2	0.5	0.05	0.4	1	0.04	0.08	1	0.04	0.08	
13	4.00e-6	0.0024	0.025	1	0.05	0.039	1	0.027	0.2	1	0.1	0.03	1	0.05	0.2	0.5	0.05	0.4	1	0.04	0.08	1	0.04	0.08	
14	5.40e-7	0.0022	0.0025	1	0.05	0.008	1	0.026	0.5	1	0.05	0.005	1	0.05	0.2	0.5	0.05	0.04	1	0.04	0.054	1	0.04	0.054	
15	1.00e-7	0.002	0.0025	1	0.05	0.008	1	0.019	0.5	1	0.05	0.005	1	0.05	0.2	0.5	0.05	0.04	1	0.04	0.054	1	0.04	0.054	
		Pu241						Pu242						Am241					Ni58			Cd			
Gr	E [MeV]	$\nu$	$\sigma_f$	$\sigma_{inel}$	$\sigma_{el}$	$\sigma_{capt}$	$\sigma_{n,2n}$	$\nu$	$\sigma_f$	$\sigma_{inel}$	$\sigma_{el}$	$\sigma_{capt}$	$\sigma_{n,2n}$	$\nu$	$\sigma_f$	$\sigma_{inel}$	$\sigma_{el}$	$\sigma_{capt}$	$\sigma_{inel}$	$\sigma_{el}$	$\sigma_{capt}$	$\sigma_{inel}$	$\sigma_{el}$	$\sigma_{capt}$	
1	7.05	0.01	0.125	0.15	0.1	0.5	0.18	0.012	0.05	0.15	0.1	0.3	0.25	0.05	0.2	0.5	0.05	0.4	0.18	0.075	0.14	0.2	0.2	0.2	
2	2.73	0.0095	0.2	0.15	0.1	0.5	0.2	0.015	0.05	0.15	0.1	0.3	1	0.05	0.2	0.5	0.05	0.4	0.14	0.2	0.085	0.2	0.2	0.2	
3	1.93	0.009	0.05	0.15	0.1	0.4	1	0.019	0.1	0.15	0.1	0.3	1	0.05	0.2	0.5	0.05	0.4	0.18	0.17	0.12	0.2	0.2	0.2	
4	8.21e-1	0.0085	0.05	0.15	0.1	0.3	1	0.02	0.1	0.15	0.1	0.3	1	0.05	0.2	0.5	0.05	0.4	0.18	0.1	0.09	0.2	0.2	0.2	
5	3.02e-1	0.008	0.06	0.2	0.1	0.2	1	0.03	0.2	0.2	0.1	0.25	1	0.05	0.2	0.5	0.05	0.4	0.16	0.04	0.09	0.2	0.2	0.2	
6	1.11e-1	0.007	0.1	0.2	0.1	0.2	1	0.0317	0.2	0.2	0.1	0.15	1	0.05	0.2	0.5	0.05	0.4	0.16	0.04	0.09	0.2	0.2	0.2	
7	4.09e-2	0.0065	0.1	0.2	0.1	0.15	1	0.0316	0.2	0.2	0.1	0.1	1	0.05	0.2	0.5	0.05	0.4	1	0.04	0.09	0.2	0.2	0.2	
8	1.50e-2	0.006	0.08	1	0.1	0.15	1	0.0315	0.2	1	0.1	0.1	1	0.05	0.2	0.5	0.05	0.4	1	0.04	0.125	0.2	0.2	0.2	
9	3.35e-3	0.0055	0.08	1	0.1	0.1	1	0.031	0.2	1	0.1	0.1	1	0.05	0.2	0.5	0.05	0.4	1	0.04	0.125	0.2	0.2	0.2	
10	7.49e-4	0.005	0.03	1	0.1	0.1	1	0.03	0.2	1	0.1	0.1	1	0.05	0.2	0.5	0.05	0.4	1	0.04	0.11	0.2	0.2	0.2	
11	4.02e-5	0.0045	0.03	1	0.1	0.1	1	0.029	0.2	1	0.1	0.09	1	0.05	0.2	0.5	0.05	0.4	1	0.04	0.11	0.2	0.2	0.2	
12	8.32e-6	0.004	0.03	1	0.1	0.1	1	0.028	0.2	1	0.1	0.08	1	0.05	0.2	0.5	0.05	0.4	1	0.04	0.1	0.2	0.2	0.2	
13	4.00e-6	0.0035	0.03	1	0.1	0.1	1	0.027	0.2	1	0.1	0.08	1	0.05	0.2	0.5	0.05	0.4	1	0.04	0.1	0.2	0.2	0.2	
14	5.40e-7	0.003	0.006	1	0.1	0.014	1	0.025	0.5	1	0.07	0.01	1	0.05	0.2	0.5	0.05	0.04	1	0.04	0.054	0.04	0.2	0.2	
15	1.00e-7	0.0024	0.006	1	0.1	0.014	1	0.02	0.5	1	0.07	0.01	1	0.05	0.2	0.5	0.05	0.04	1	0.04	0.054	0.04	0.2	0.2	
		U238						U235						Pb				Na			Cr52			H	
Gr	E [MeV]	$\nu$	$\sigma_f$	$\sigma_{inel}$	$\sigma_{el}$	$\sigma_{capt}$	$\sigma_{n,2n}$	$\nu$	$\sigma_f$	$\sigma_{inel}$	$\sigma_{el}$	$\sigma_{capt}$	$\sigma_{n,2n}$	$\sigma_{inel}$	$\sigma_{el}$	$\sigma_{capt}$	$\sigma_{n,2n}$	$\sigma_{inel}$	$\sigma_{el}$	$\sigma_{capt}$	$\sigma_{inel}$	$\sigma_{el}$	$\sigma_{capt}$	$\sigma_{el}$	$\sigma_{capt}$
1	7.05	0.01	0.0263	0.19	0.05	0.3	0.07	0.007	0.025	0.05	0.08	0.15	0.07	0.4	0.2	0.2	1	0.3	0.06	0.15	0.41	0.075	0.15	0.35	0.35
2	2.73	0.015	0.0225	0.095	0.05	0.1	0.09	0.0065	0.02	0.05	0.08	0.12	0.09	0.4	0.2	0.2	1	0.3	0.06	0.1	0.06	0.04	0.18	0.35	0.35
3	1.93	0.016	0.019	0.07	0.05	0.03	1	0.006	0.02	0.05	0.08	0.12	1	0.4	0.2	0.2	1	0.3	0.06	0.07	0.085	0.025	0.2	0.35	0.35
4	8.21e-1	0.018	0.036	0.05	0.05	0.0325	1	0.0055	0.02	0.1	0.08	0.07	1	0.4	0.2	0.2	1	0.4	0.06	0.07	0.15	0.12	0.17	0.35	0.35
5	3.02e-1	0.02	0.146	0.066	0.05	0.0253	1	0.005	0.02	0.1	0.08	0.07	1	0.4	0.2	0.2	1	0.4	0.06	0.07	0.09	0.15	0.1	0.35	0.35
6	1.11e-1	0.03	0.2	0.072	0.05	0.022	1	0.0045	0.02	0.1	0.08	0.07	1	0.4	0.2	0.2	1	1	0.06	0.07	1	0.15	0.1	0.35	0.35
7	4.09e-2	0.031	0.2	0.07	0.05	0.019	1	0.004	0.015	0.15	0.08	0.07	1	0.4	0.2	0.2	1	1	0.06	0.07	1	0.15	0.1	0.35	0.35
8	1.50e-2	0.03	0.2	1	0.05	0.018	1	0.0035	0.015	0.15	0.08	0.07	1	0.4	0.2	0.2	1	1	0.06	0.07	1	0.15	0.1	0.35	0.35
9	3.35e-3	0.029	0.3	1	0.05	0.024	1	0.0032	0.015	0.15	0.08	0.07	1	0.4	0.2	0.2	1	1	0.06	0.07	1	0.15	0.1	0.35	0.35
10	7.49e-4	0.028	0.3	1	0.05	0.024	1	0.003	0.015	1	0.06	0.07	1	0.4	0.2	0.2	1	1	0.05	0.06	1	0.15	0.1	0.35	0.35
11	4.02e-5	0.027	0.3	1	0.05	0.029	1	0.0025	0.03	1	0.06	0.07	1	0.4	0.2	0.2	1	1	0.05	0.06	1	0.15	0.1	0.35	0.35
12	8.32e-6	0.0265	0.3	1	0.05	0.02	1	0.0022	0.03	1	0.06	0.05	1	0.4	0.2	0.2	1	1	0.05	0.06	1	0.15	0.1	0.35	0.35
13	4.00e-6	0.026	0.3	1	0.05	0.01	1	0.002	0.03	1	0.06	0.05	1	0.4	0.2	0.2	1	1	0.04	0.06	1	0.15	0.1	0.35	0.35
14	5.40e-7	0.025	0.22	1	0.01	0.006	1	0.0016	0.002	1	0.04	0.0075	1	0.04	0.2	0.2	1	1	0.02	0.075	1	0.04	0.079	0.35	0.35
15	1.00e-7	0.02	0.22	1	0.01	0.006	1	0.0014	0.002	1	0.035	0.0075	1	0.04	0.2	0.2	1	1	0.02	0.075	1	0.04	0.079	0.35	0.35